# Effect of Incorporated CdS Nanoparticles on the Crystallinity and Morphology of Poly(styrene-*b*-ethylene oxide) Diblock Copolymers

SIAO-WEI YEH,[1] TZUNG-LUEN WU,[1] KUNG-HWA WEI,[1] YA-SEN SUN,[2] KENG S. LIANG[2]

[1]Department of Materials Science and Engineering, National Chiao Tung University, Hsinchu, Taiwan 30049, Republic of China

[2]National Synchrotron Radiation Research Center, 101 Hsin-Ann Road, Science-Based Industrial Park, Hsinchu, Taiwan 30077, Republic of China

*Received 23 March 2004; revised 11 August 2004; accepted 3 January 2005*
*DOI: 10.1002/polb.20417*
*Published online in Wiley InterScience (www.interscience.wiley.com).*

**ABSTRACT:** Surface-modified CdS nanoparticles selectively dispersed in hexagonally packed poly(ethylene oxide) (PEO) cylinders of poly(styrene-*b*-ethylene oxide) (PSEO) block copolymers were prepared. The photoluminescence and ultraviolet–visible characteristics of the presynthesized CdS nanoparticles in *N*,*N*-dimethylformamide and in PEO domains of the PSEO block copolymers were determined. Because of strong interactions between the CdS nanoparticles and PEO chains, as shown by Fourier transform infrared spectroscopy, the incorporation of the CdS nanoparticles prevented the PEO cylinders from properly crystallizing; this was confirmed by differential scanning calorimetry and wide-angle X-ray diffraction measurements. The intercylinder distance between the swollen and reduced-crystallinity CdS/PEO cylinders in turn increased, as confirmed by small-angle X-ray scattering and transmission electron microscopy. At a high CdS concentration (43 wt % or 8.3 vol % with respect to PEO), however, the hexagonally packed cylindrical nanostructure of the PSEO diblock copolymers was destroyed.  J Polym Sci Part B: Polym Phys 43: 1220–1229, 2005
**Keywords:** block copolymers; cadmium sulfide; poly(styrene-*b*-ethylene oxide)

## INTRODUCTION

Block copolymers are versatile platform materials because they can self-assemble into various nanostructures with periodic thicknesses on the scale of tens to hundreds of nanometers under the appropriate compositions and conditions on account of microphase separation between incompatible blocks.[1–4] The crystallization and morphology of one particular class of block copolymers, crystalline–amorphous diblock copolymers, have been studied extensively. For example, the morphology and crystallization of asymmetric poly(styrene-*b*-ethylene oxide) (PSEO),[5,6] poly(1,4-butadiene)-*b*-poly(styrene-*r*-butadiene), polyethylene-*b*-poly(vinylcyclohexane),[7] and poly(butadiene-*b*-ethylene oxide)[8,9] have been reported. On the other hand, a number of studies involving nanostructured block copolymers for nanomasks in lithography,[10,11] nanotemplate,[12–21] and photonic crystal[22] applications have been reported recently. For instance, ordered Ti/Au,[10] Si, Co,[11] and silicon nitride arrays have been fabricated with block copolymer lithography. Additionally, Au and Ag nanowire[12] and CdSe

*Correspondence to:* K.-H. Wei (E-mail: khwei@cc.nctu.edu.tw)

and Co nanowire arrays[13] have been produced with polystyrene-*b*-poly(methyl methacrylate) (PS-*b*-PMMA) block copolymers as templates. In other cases, quasi-regular arrays of Au clusters[14] and self-assemblies of both Au and $Fe_2O_3$ nanoparticles[15] have been synthesized with micellar polystyrene-*b*-poly(vinylpyridine) (PS-*b*-PVP). The groups of Cohen[16] and Schrock[17] have reported the synthesis of Mn-doped and Tb-doped ZnS, iron–cobalt, iron–nickel, $Fe_2O_3$, PbS, ZnS, and CdSe nanoparticles in block copolymers by organometallic complexes. Several groups have also reported the *in situ* synthesis of $CoFe_2O_4$[18] and CdS[19] nanoparticles or the ability to control the spatial location of nanoparticles such as Au and $SiO_2$,[20] Pd,[21], $TiO_2$, and CdS[22] by polystyrene-*b*-poly(ethylene propylene), polystyrene-*b*-poly(acrylic acid), PS-*b*-PMMA, PS-*b*-PVP, and PSEO, respectively.

The use of nanostructured block copolymers as templates to selectively control the spatial position of semiconductor nanoparticles in one of the blocks may lead to several potential applications.[23,24] For instance, periodic high-refractive-index contrast domains in phase-separated block copolymers can be used in photonic crystal applications.[23] Nanoparticles with highly efficient luminescence can be combined with organic layers in light-emitting devices.[24] The incorporation of nanoparticles into block copolymers, however, would lead to more complicated morphologies with respect to their pristine state, as theoretically predicted by the group of Balazs:[25] they used self-consistent field theory and density functional theory to describe the structure of the polymer and the nanoparticles, respectively, and predicted the morphology and their phase diagrams. Recently, we have adopted an approach to synthesize $TiO_2$ and CdS nanoparticles via the attachment of various surface ligands. These surfactants can be either hydrophilic or hydrophobic and tethered to $TiO_2$ and CdS nanoparticles by an ionic or covalent bond. Selective dispersions of surface-modified $TiO_2$ in the polystyrene (PS) or poly(methyl methacrylate) domains of PS-*b*-PMMA[22(a)] and CdS in the poly(ethylene oxide) (PEO) domains of PSEO[22(b)] have been obtained. This selectivity leads to a change in the morphology of the block copolymer. For instance, the incorporation of CdS nanoparticles into the PEO domain of 125,000PS-*b*-16,100PEO results in a morphological transformation forming a body-centered-cubic or simple cubic nanostructure.[22(b)] Moreover, the evolution of the size distribution of CdS nanoparticles, from *N,N*-dimethylformamide (DMF) solutions to the final polymer composites, has been reported in detail and measured by small-angle X-ray scattering (SAXS) in an absolute intensity scale.[22(c)] The binding of CdS nanoparticles promotes the segregation of the PEO and nanoparticles and leads to spherical CdS/PEO microdomains in the composite film with greatly enhanced thermal stability.

In this study, we prepared hexagonally packed cylindrical (HEX) CdS/PSEO nanocomposites with lower molecular weight PSEO. The effects of the CdS nanoparticle concentration on the crystallization and morphology of PSEO diblock copolymers are reported in detail. Moreover, we have determined the characteristics of presynthesized CdS nanoparticles in an organic solvent, DMF, and in PEO domains of PSEO block copolymers with ultraviolet–visible (UV–vis) absorption spectra and photoluminescence (PL).

## EXPERIMENTAL

Cadmium acetate dihydrate [$Cd(Ac)_2{\cdot}2H_2O$], sodium sulfide ($Na_2S{\cdot}9H_2O$), and mercaptoethanol ($HSC_2H_4OH$) were purchased from Aldrich. A PSEO diblock copolymer with a molecular weight of 19,000PS/12,600PEO was purchased from Polymersource, Inc. CdS nanoparticles were synthesized with $HSC_2H_4OH$ as the surfactant through the reaction of $Cd(Ac)_2{\cdot}2H_2O$, $Na_2S{\cdot}9H_2O$, and $HSC_2H_4OH$ in methanol with a modification of the kinetic trapping method.[26] The synthetic steps have been reported in detail elsewhere.[22(b),26(b,c)] The surfactant-modified

**Table 1.** Characteristic Properties of CdS Nanoparticles

| $\lambda^{a}_{edge}$ | $\lambda^{b}_{max}$ | $2R^{c}_{edge}$ | $2R^{d}_{max}$ | RPI[e] | Crystal Size[f] |
|---|---|---|---|---|---|
| 445 nm | 360 nm | 3.4 nm | 2.0 nm | 1.12 | 1.33 nm |

[a] The edge absorption wavelength of CdS nanoparticles in DMF as obtained from UV–vis spectra in Figure 1(a).
[b] The absorption wavelength of the mode of CdS nanoparticles.
[c] The larger size of CdS nanoparticles was calculated with $\lambda_{edge}$ from UV–vis spectra with 1.[19,26,27]
[d] The mode of the CdS size was calculated from $\lambda_{max}$.
[e] RPI was determined with eq. 3.[19]
[f] The crystal size was calculated with the Debye–Scherrer equation.

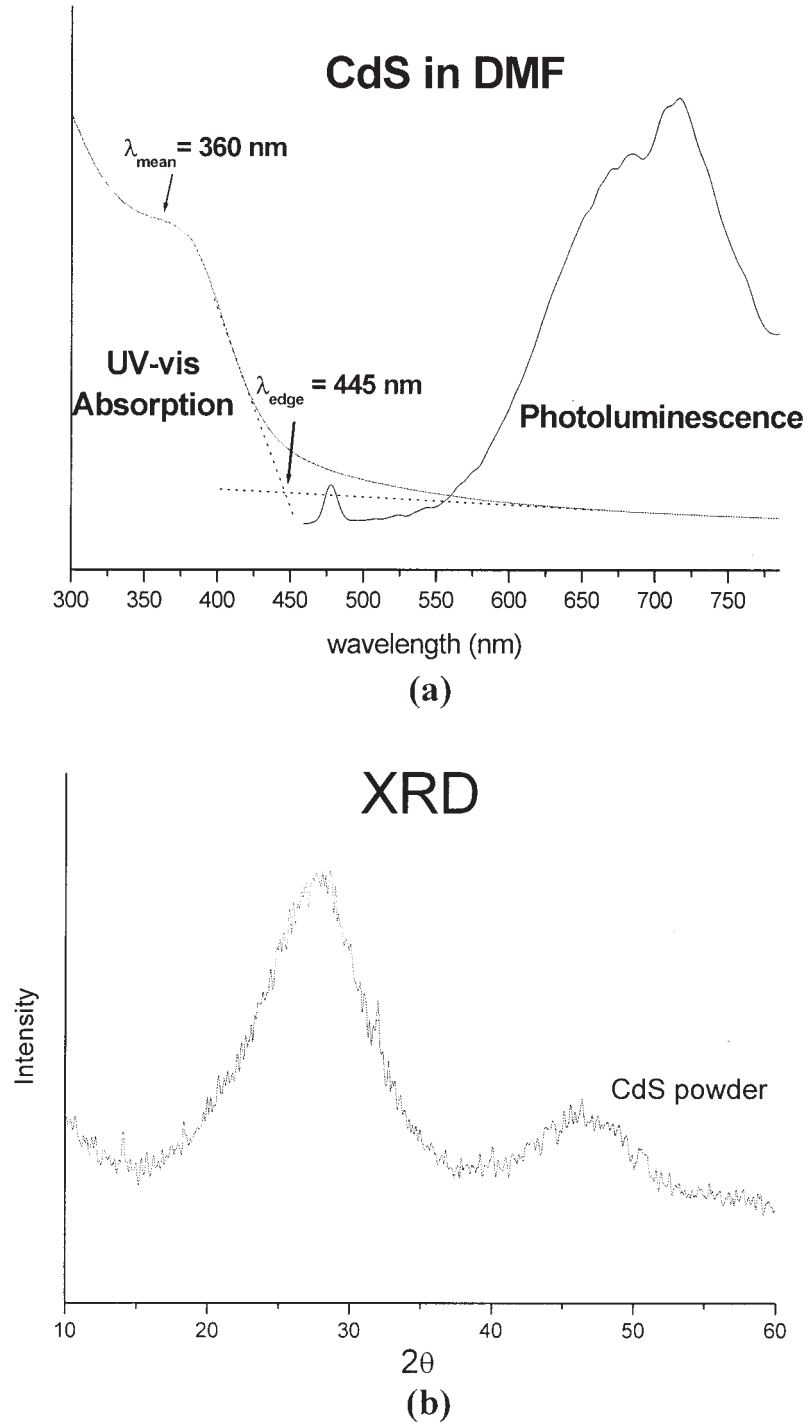


**Figure 1.** (a) UV–vis absorption and PL spectra of CdS capped with $HSC_2H_4OH$ in DMF and (b) X-ray diffraction curve of CdS powder.

CdS, containing a chemically active hydroxyl surface, became hydrophilic. The basic properties were determined and are listed in Table 1. In Table 1, two kinds of CdS sizes, $2R_{edge}$ and $2R_{max}$, calculated individually from edge absorption wavelengths $\lambda_{edge}$ and $\lambda_{max}$ in the UV–vis spectrum of Figure 1(a), typically represent the larger size and mode size in the size distribution curve of CdS in DMF.[19,26] The CdS size obtained from X-ray diffraction is the crystal size and represents the smallest size; this corresponds to the fact that we have polycrystalline CdS.

Subsequently, CdS/DMF was added to a previously prepared PSEO/DMF solution with stirring. This mixture was dried slowly *in vacuo* at 323 K and then maintained at 383 K for 24 h; afterwards, the CdS/PSEO nanocomposite film was obtained. The preparation of the pure PSEO films was similar. Thermogravimetric analysis was used to ensure that no residual DMF solvent was present.

## Characterization

SAXS experiments were performed on the BL-17B1 wiggler beam line at the National Synchrotron Radiation Research Center of Taiwan. UV–vis absorption spectra of a CdS-containing solution in a quartz cell and CdS-containing block copolymer films were recorded on an Aglient 8453 UV–vis spectrometer with scanning between 200 and 1000 nm. PL spectra were obtained with a Hitachi F4500 fluorescence spectrophotometer at room temperature. Wide-angle X-ray diffraction (WAXD) measurements on the samples were collected with a conventional rotating-anode source. Fourier transform infrared (FTIR) spectra of the samples were obtained with a Nicolet Protégé-460 spectrometer. Transmission electron microscopy (TEM) was performed on a Hitachi H-600 instrument operating at 100 kV; ultrathin sections of CdS/PSEO nanocomposites for TEM studies were microtomed with a Leica Ultracut Uct equipped with a diamond knife and were subsequently deposited on copper grids. The glass-transition temperatures ($T_g$'s) and melting points ($T_m$) of the bulk films were obtained with a Dupont DSC 2910 instrument at a heating rate of 20 °C/min.

Figure 1(a) shows UV–vis absorption and PL spectra of the CdS nanoparticles. In the UV–vis absorption spectrum, a blueshift (68 nm) in the absorption edge (447 nm) with respect to the bulk value (515 nm) and the appearance of an exciton shoulder and a blueshift of the absorption edge indicate that the CdS nanoparticles were quantum-confined.[19,26(a)] From the absorption wavelength, the size of the CdS nanoparticles was calculated as follows:[26(d)]

$$E_{g_{abs}} - E_{g_{ref}} = \Delta E_g \approx \frac{\eta^2\pi^2}{2R^2}\cdot\frac{1}{\mu} - \frac{1.8e^2}{\varepsilon R} \qquad (1)$$

where $E_{g_{abs}}$ is the energy gap of quantum confined CdS nanoparticles, $E_{g_{ref}}$ is the energy gap of bulk CdS, $\Delta E_g$ is the difference between energy gap of bulk and quantum confined CdS, $R$ is the radius of the particle, $\mu$ is the reduced mass of the exciton (i.e., $\mu^{-1} = m_h^{*-1} + m_e^{*-1}$, where $m_e^{*-1}$ is the effective mass of the electron and $m_h^{*-1}$ is the effective mass of the hole), and ε is the dielectric constant of the material. From the UV–vis absorption spectrum, two CdS sizes (3.4 nm for $2R_{edge}$ and 2.0 nm for $2R_{max}$), as listed in Table 1, were calculated individually from edge absorption wavelengths $\lambda_{edge}$ and $\lambda_{max}$. $\lambda_{edge}$ and $\lambda_{max}$ correspond to the larger mean particle size and the mode size in a size distribution, respectively. The sizes of CdS in DMF, determined by the energy gaps of semiconductors from UV–vis absorption spectra, were consistent with those calculated by SAXS in an absolute intensity scale in our previous studies.[22(c)] The polydispersity of the sample was assessed by the calculation of the half-width of the size distribution ($d_{1/2}$), 1.4 nm, which is defined as follows:

$$d_{1/2} = 2R_{edge} - 2R_{max} \qquad (2)$$

If we assume a Gaussian distribution of particles, the $d_{1/2}$ value can be taken to be twice that of the standard deviation ($\sigma_{2R}$), and $2R_{max}$ approximates the mean particle diameter ($2R_{mean}$). Then, a simplified radius polydispersity index (RPI) can be defined as follows:[19]

$$\mathrm{RPI} = (\sigma_{2R}/2R_{mean})^2 + 1 \qquad (3)$$

As shown in Table 1, RPI for the CdS nanoparticles in this case was approximately 1.12.

PL of CdS in DMF, as shown in Figure 1(a), exhibited a sharp excitonic fluorescence at 478 nm and two broad peaks at 683 and 717 nm, which were due to two different states of surface trapping.[26(a),27] Fluorescence by surface-trapped states, which is exhibited by most nanoparticles, results from nonradiative decay of the free electrons to the deep-trapped state; it does not indicate a high agglomeration of CdS nanoparticles. In this study, the intensity of the surface-trapped fluorescence was much stronger than that of the excitonic fluorescence, and this indicated poor passivation of the surface state of the CdS nanoparticles. This could have been caused by the defects of CdS nanocrystals or the surface modification by $HSC_2H_4OH$.[26(a),27]

Figure 1(b) shows X-ray diffraction curves of the CdS powders; they have broad peaks ($2\theta$ = 20–40°) associated with their sphalerite structure. In the case of spherical crystallites, the relationship between the coherence length ($L$) and the

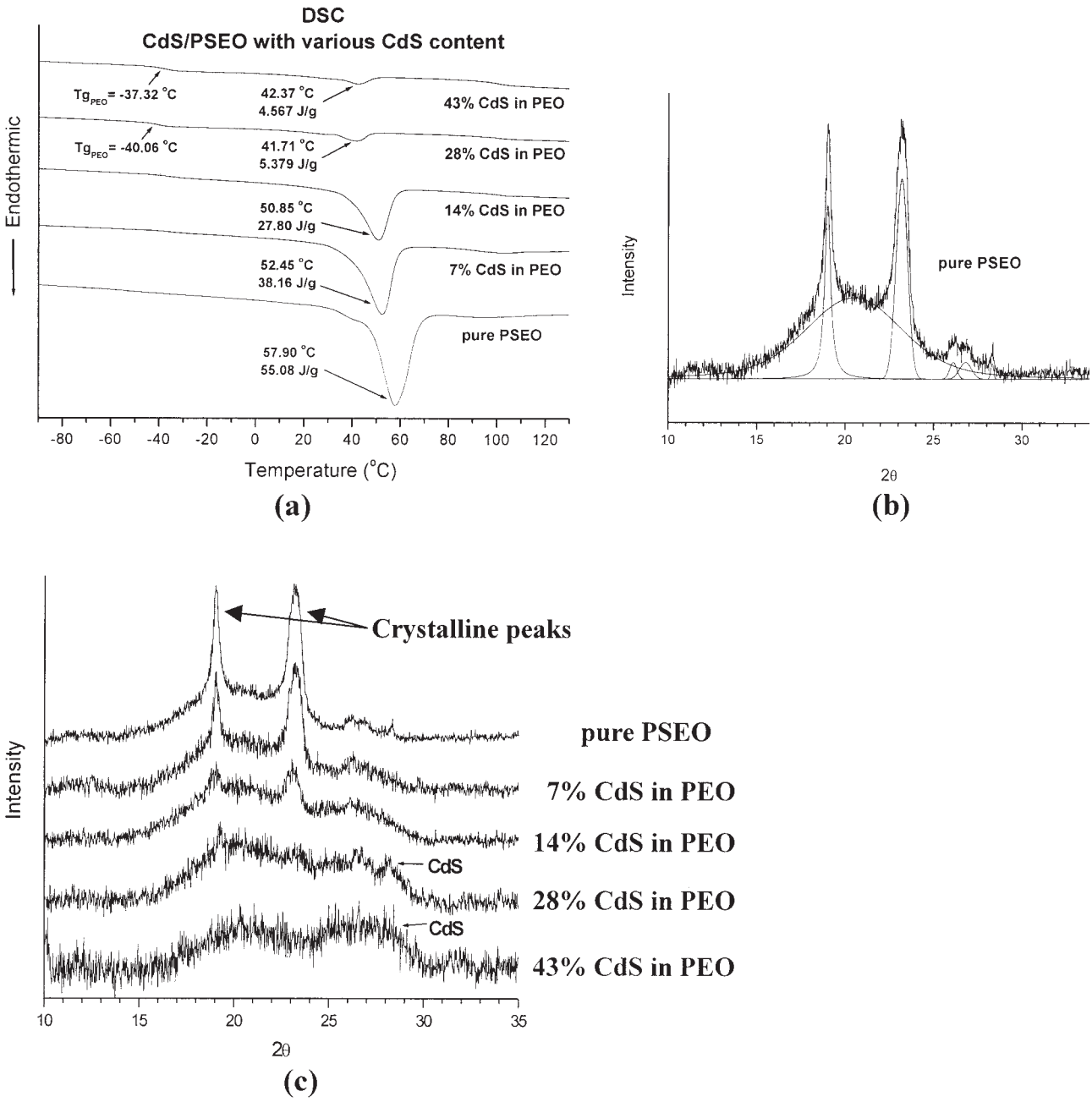


**Figure 2.** (a) DSC and (b,c) X-ray diffraction curves of CdS/PSEO with various CdS nanoparticle concentrations.

diameter of CdS ($D$) is given by $L = 3/4D$. $L$ was calculated with the Debye–Scherrer formula:

$$L = \frac{0.9\lambda}{B\cos\theta} \tag{4}$$

where $B$ is the full width at half-maximum of the peak, $\lambda$ is the X-ray wavelength, and $\theta$ is the angle of diffraction. The crystal size of CdS determined by this method was 1.33 nm. The CdS size obtained from X-ray diffraction was the crystal size and represented the smallest size; this corresponded to the fact that we had polycrystalline CdS.

## RESULTS AND DISCUSSION

Figure 2(a) shows differential scanning calorimetry (DSC) analysis results for CdS/PSEO with

**Table 2.** Crystallinity of CdS/PEO Composites with Various CdS Concentrations from DSC and WAXD Results

| CdS/PSEO | $X_c^{DSCa}$ | $X_c^{WAXDb}$ |
|---|---|---|
| 0% CdS in PEO | 0.69 | 0.72 |
| 7% CdS in PEO | 0.48 | 0.53 |
| 14% CdS in PEO | 0.35 | 0.28 |
| 28% CdS in PEO | 0.07 | 0.13 |
| 43% CdS in PEO | 0.06 | 0.00 |

[a] $X_c^{DSC}$ was calculated from DSC curves with eq. 5.
[b] $X_c^{WAXD}$ was calculated from WAXD curves after deconvolution with eq. 6.

various amounts of incorporated CdS nanoparticles. A crystal melting peak at 58 °C associated with the PEO domain ($T_{mPEO}$) appears in the pure PSEO case, whereas the glass-transition temperature of the amorphous phase of PEO ($T_{gPEO}$) is undetectable. In the presence of 43% CdS nanoparticles, the crystallinity of the PEO domain decreases to 5 J/g from 55 J/g for the pure PEO domain, and $T_{mPEO}$ decreases to 42 °C from 58 °C for pure PEO in PSEO. $T_{gPEO}$ is −40 °C as the CdS concentration increases. The crystallinity ($X_C^{DSC}$) can be calculated from the DSC curves as follows:

$$X_C^{DSC} = \frac{1}{w_{EO}}\left(\frac{\Delta H}{\Delta H_0}\right) \quad (5)$$

where $w_{EO}$ is the weight fraction of PEO, $\Delta H$ is the heat of fusion calculated from the melting peak in DSC, and $\Delta H_0$ is the heat of fusion for completely crystallized PEO ($\Delta H_0$ = 200 J/g),[28] as shown in Table 2. This indicates that CdS dispersed in the PEO domains in PSEO hinders the crystallization of PEO domains. Moreover, the WAXD results also support the corresponding crystal-to-amorphous change of the PEO domain in PSEO. Figure 2(b) shows the WAXD curves of pure PSEO after deconvolution; two sharp peaks at $2\theta$ values of 19.0 and 23.21° represent the crystalline peaks of the PEO domain. The WAXD curves in Figure 2(c) can be deconvoluted to determine the crystallinity ($X_C^{WAXD}$), and the results are given in Table 2. $X_C^{WAXD}$ can be obtained as follows:

$$X_C^{WAXD} = \frac{1}{w_{EO}}\left(\frac{A_c}{A_c + A_a}\right) \quad (6)$$

where $A_c$ and $A_a$ are the areas under the crystalline and amorphous peaks. The CdS diffraction peak has been deconvoluted and taken out from the PEO crystalline curves. This analysis shows that the crystallinity of the PEO domain decreases with an increasing amount of CdS, and this indicates the retardation of PEO crystallization by the CdS nanoparticles. This result is also consistent with those obtained by DSC. The decrease in the crystallinity of the PEO domain and the loading of CdS nanoparticles lead to the swelling of the CdS/PEO composite cylinders and an increase in the volume fraction of the CdS/PEO domain in PSEO.

To verify the intermolecular interactions between the CdS nanoparticles and PEO block, the vibration spectra of CdS/PSEO in a selected region [C—O—C symmetric and asymmetric stretching (1200–1000 $cm^{-1}$)] were obtained, as shown in Figure 3, and the results are discussed in the following. In the presence of 7–43% CdS in the PEO domains, the C—O—C stretch vibrations of PEO chains display a shift toward lower wave numbers, from 1100 to 1085 $cm^{-1}$. The changes in the intensity, shape, and position of the C—O—C stretching mode are associated with the interaction between PEO and surface-hydroxylated CdS nanoparticles, and they reveal the formation of dipole–dipole interactions between the oxygen atoms of PEO chains and hydroxyl groups on CdS nanoparticles.[29]

Figure 4 shows one-dimensional SAXS patterns of CdS/PSEO nanocomposites with various CdS concentrations by synchrotron radiation. For pure PSEO, four peaks appear at $Q$ values

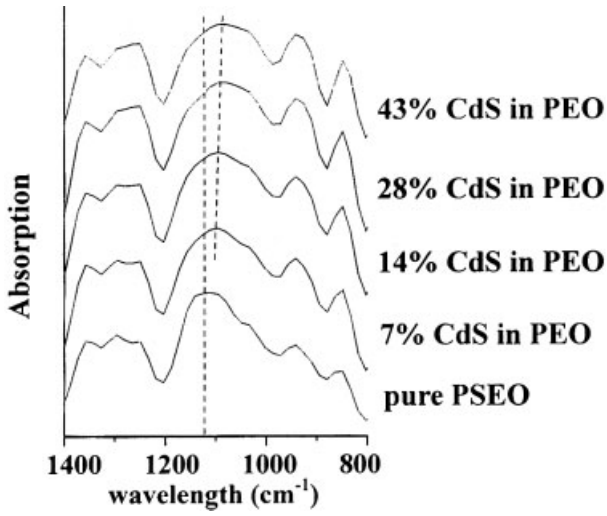


**Figure 3.** FTIR spectra of CdS/PSEO in a selected region: C—O—C symmetric and asymmetric stretching (1200–1000 $cm^{-1}$).

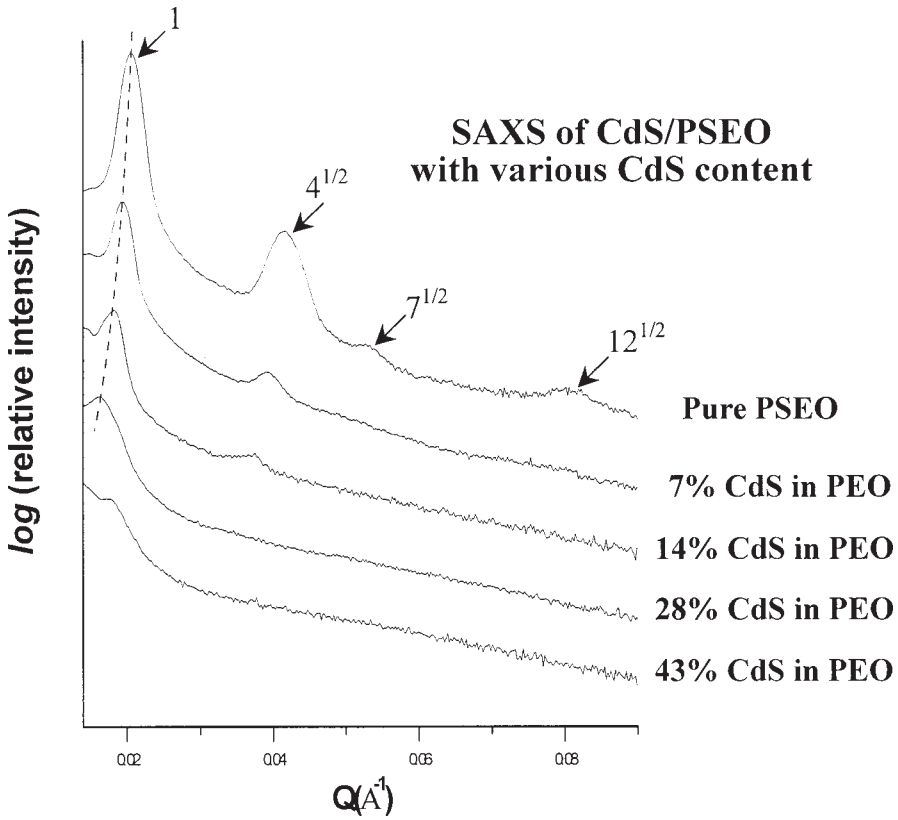


**Figure 4.** SAXS of CdS/PSEO nanocomposites with various CdS nanoparticle concentrations.

of 0.021, 0.041, 0.053, and 0.078 $Å^{-1}$, which correspond to a ratio of $1:4^{1/2}:7^{1/2}:12^{1/2}$ ($Q = 4\pi \sin(\theta)/\lambda$, $\lambda$ is the wavelength of X-ray). This ratio indicates scattering by HEX nanostructures. The intercylinder distance ($D$) was determined to be 35.07 nm as follows:

$$D = (4/3)^{1/2} \times d_{100} \qquad (7)$$

where $d_{100}$ is equal to $2\pi/Q_{100}$ and $Q_{100}$ is 0.21 $nm^{-1}$ ($Q_{100}$ is the scattering peak caused by the HEX structure factor). After the incorporation of CdS nanoparticles into the PSEO diblock copolymer, HEX nanostructures in CdS/PSEO still remain, but the ordering peaks of SAXS curves shift to a lower $Q$ region; this indicates an enlargement of the center-to-center distance between the PEO composite cylinders. The distance is measured from the center of a cylinder to that of a neighboring cylinder. The enlarged distance is a result of the reduced crystallinity and swollen CdS/PEO composite cylinders. A complete listing of intercylinder distances for various CdS/PSEO nanocomposites is given in Table 3. According to the SAXS curves, an increasing CdS concentration in PSEO leads to a reduction in the ordering peaks because of the convolution with CdS nanoparticle scattering contributions. For CdS/PSEO with 43% CdS in the PEO block, the HEX PEO nanostructure is destroyed, and this may be explained by the fact that CdS nanoparticles fill up a large fraction of free spacing in the PEO domains and alter the surface energy of the PEO composite domains in PSEO.

Figure 5 shows TEM images of PSEO containing various amounts of CdS nanoparticles.

**Table 3.** SAXS Results for CdS/PSEO with Various CdS Concentrations

| CdS/PSEO | $Q_{100}$ ($nm^{-1}$)[a] | $d_{100}$ (nm)[b] | $D$ (nm)[c] |
|---|---|---|---|
| 0% CdS in PEO | 0.21 | 30.37 | 35.07 |
| 7% CdS in PEO | 0.19 | 32.40 | 37.42 |
| 14% CdS in PEO | 0.18 | 34.66 | 40.02 |
| 28% CdS in PEO | 0.16 | 38.79 | 44.79 |
| 43% CdS in PEO | — | — | — |

[a] $Q_{100}$ was determined from SAXS curves in Figure 4.
[b] $d_{100}$ was calculated as follows: $d_{100} = 2\pi/Q_{100}$.
[c] The intercylinder distance ($D$) was calculated with eq. 5.

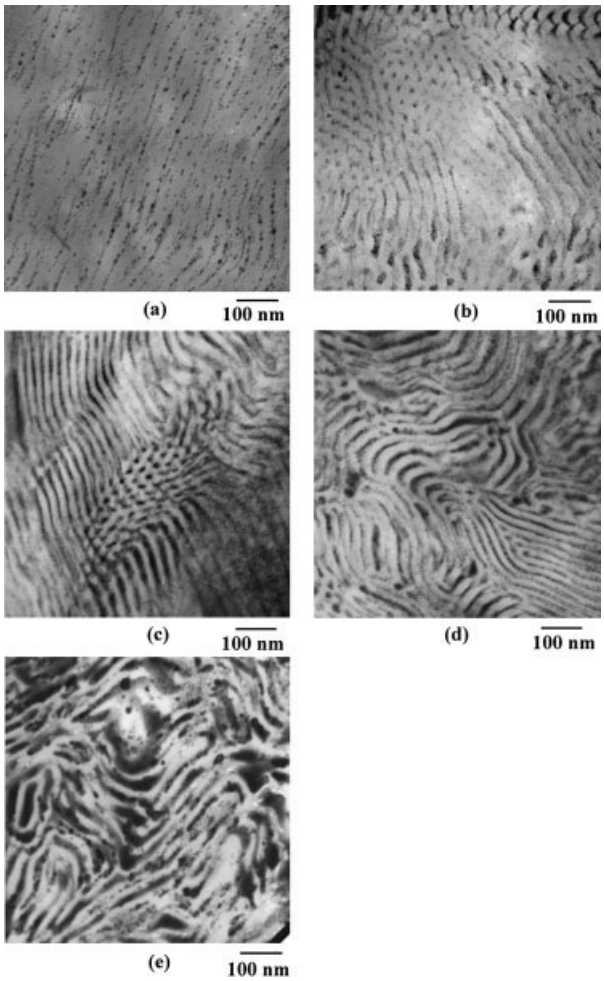


**Figure 5.** TEM images of (a) PSEO stained with $OsO_4$, (b) 7% CdS nanoparticles in PEO of PSEO, (c) 14% CdS nanoparticles in PEO of PSEO, (d) 28% CdS nanoparticles in PEO of PSEO, and (e) 43% CdS nanoparticles in PEO of PSEO.

In Figure 5(a), the dark region, due to staining by $OsO_4$, is the PEO domain, and the lighter region is the PS domain. The cylindrical nanostructure of pure PSEO is easily revealed. The diameter of the PEO cylinder is approximately 14 nm. There is no staining in Figure 5(b–f); the darker color represents the PEO/CdS composite phase because of the higher electron density of cadmium. The location of CdS in the PEO domain has been probed by energy-dispersive spectrometry, and no PEO domains without CdS nanoparticles have been observed in PSEO. The selective distribution of $HSC_2H_4OH$-modified CdS in the PEO domain is likely due to dipole–dipole interactions between the hydroxyl groups of $HSC_2H_4OH$ and the PEO block. In Figure 5(b–e), the cylindrical morphology of CdS/PSEO nanocomposites is distorted when the concentration of CdS nanoparticles in the PEO phase is increased. The cylindrical nanostructure, however, is destroyed in high-CdS-concentration CdS/PSEO (43% CdS in PEO), as shown in Figure 5(f), and this is consistent with SAXS results.

Figure 6 compares PL properties of CdS in DMF and in PEO domains. After the selective dispersion of CdS in the PEO domains of the PSEO block copolymer, the excitonic fluorescence diminishes, and apparent red and broad surface-trapped luminescent characteristics remain largely unchanged. Moreover, the main broad surface-trapped fluorescence of CdS nanoparticles in PEO domains displays a slight blueshift to 711 nm from 717 nm when the CdS concentration is low (7–28%), but it displays a redshift to 715 nm with a 43% CdS concentration in PEO. The disappearance of the excitonic fluorescence and the blueshift of the broad surface-trapped fluorescence can be explained by the fact that the chemical environment of the CdS nanoparticles has changed from amide groups (in DMF) to ethylene oxide groups (in PEO blocks). With a high CdS concentration (43%) in the PEO domains, however, the CdS nanoparticles become agglomerated in the PEO domains and cause the redshift of the surface-trapped fluorescence.

To clarify the agglomeration of CdS nanoparticles in DMF and in the composites, we examined in more detail the surfactant removal and its sequence in the process. The surface-hydroxylated CdS nanoparticles were synthesized by the bonding of the surfactant, $HSC_2H_4OH$, to CdS nanoparticles with the thiol group, and then they were dispersed and mixed with PSEO in DMF. The CdS/SEO nanocomposite films were formed after they were dried *in vacuo* at 323 K and kept at 383 K for 24 h. During the drying processes, the solvent, DMF, was removed and, in our opinion, a small amount of $HSC_2H_4OH$ may also have been carried away from the CdS surface because of the strong hydrogen bonding between DMF and $HSC_2H_4OH$ and the lower boiling point of $HSC_2H_4OH$ in comparison with that of DMF (157 vs. 165 °C). The removal of the surfactant from the surface of the CdS nanoparticles caused their agglomeration and the broadening and redshift of their PL peaks. By comparing PL of CdS/PSEO composites and that of CdS in DMF, we found that the amount of the surfactant that was

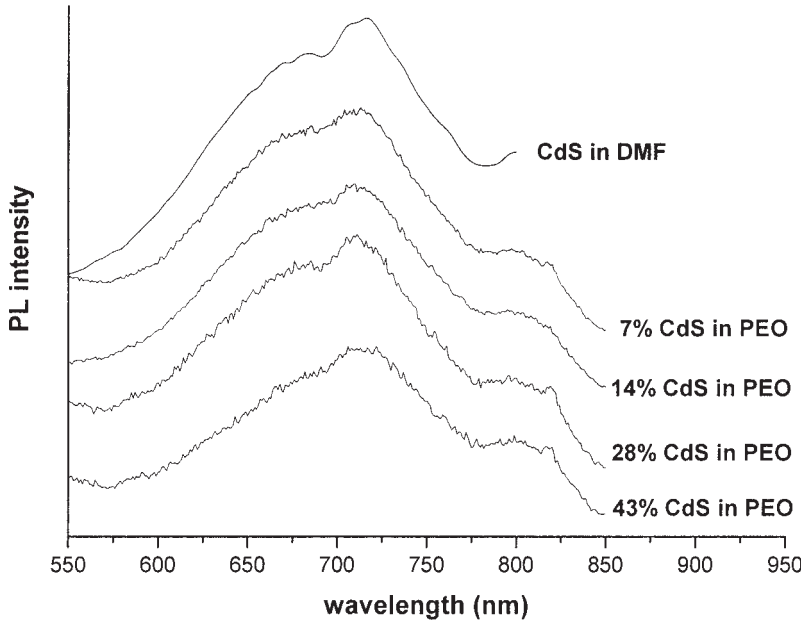


**Figure 6.** PL spectra of CdS nanoparticles in DMF and CdS/PSEO with various CdS nanoparticle concentrations.

removed was apparently small during the drying processes because no redshift, only a little broadening, is shown in the PL peaks in Figure 6.

## CONCLUSIONS

CdS/PSEO nanocomposites with selective dispersions of surface-modified CdS nanoparticles in hexagonally packed PEO cylinders of PSEO block copolymers have been prepared. CdS nanoparticles hinder the crystallization of PEO and result in an increase in the intercylinder distance of HEX CdS/PSEO, as shown in Scheme 1. A high CdS nanoparticle concentration, however, destroys the ordered HEX nanostructure of PSEO. The size and RPI of CdS have been determined from UV–vis absorption spectra, and a comparison of PL of CdS in DMF and in PEO domains of PSEO block copolymers has been discussed in detail.

The authors appreciate the financial support of the National Science Council through project NSC 92-2120-M-009-009.

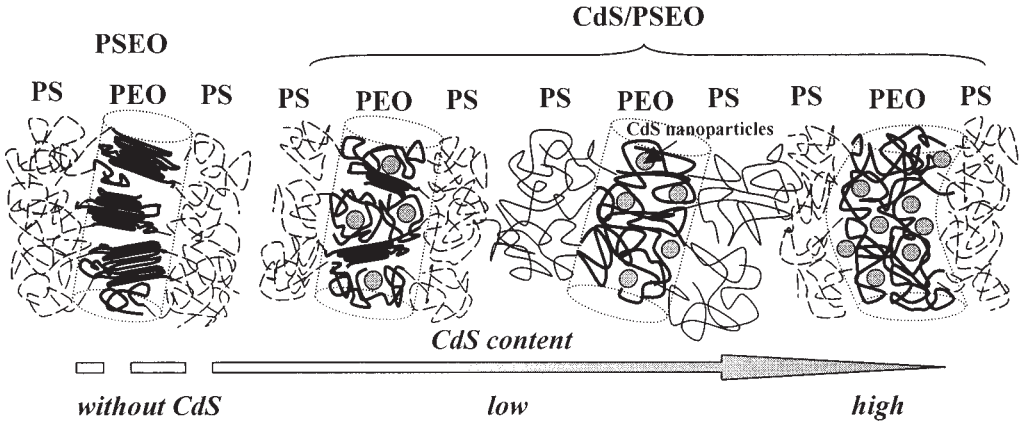


**Scheme 1.** Crystalline and morphological properties of CdS/PSEO with various CdS concentrations.

## REFERENCES AND NOTES


1. (a) Bates, F. S.; Fredrickson, G. H. Annu Rev Phys Chem 1990, 41, 525; (b) Bates, F. S. Science 1991, 251, 898.
2. Hamley, I. W. The Physics of the Block Copolymers; Oxford University Press: New York, 1998.
3. Lazzari, M.; Lopez-Quintela, M. A. Adv Mater 2003, 15, 1583.
4. Park, C.; Yoo, J.; Thomas, E. L. Polymer 2003, 44, 6725.
5. (a) Zhu, L.; Huang, P.; Chen, W. Y.; Weng, X.; Cheng, S. Z. D.; Ge, Q.; Quirk, R. P.; Senador, T.; Shaw, M. T.; Thomas, E. L.; Lotz, B.; Hsiao, B. S.; Yeh, F.; Liu, L. Macromolecules 2003, 36, 3180; (b) Zhu, L.; Cheng, S. Z. D.; Huang, P.; Ge, Q.; Quirk, R. P.; Thomas, E. L.; Lotz, B.; Hsiao, B. S.; Yeh, F.; Liu, L. Adv Mater 2002, 14, 31.
6. Li, L.; Serero, Y.; Koch, M. H. J.; de Jeu, W. H. Macromolecules 2003, 36, 529.
7. (a) Loo, Y. L.; Register, R. A.; Ryan, A. J. Macromolecules 2002, 35, 2365; (b) Loo, Y. L.; Register, R. A.; Ryan, A. J.; Dee, G. T. Macromolecules 2001, 34, 8968.
8. (a) Rottele, A.; Thurn-Albrecht, T.; Sommer, J. U.; Reiter, G. Macromolecules 2003, 36, 1257; (b) Reiter, G.; Castelein, G.; Sommer, J. U.; Rottele, A.; Thurn-Albrecht, T. Phys Rev Lett 2001, 87, 226101.
9. Chen, H. L.; Hsiao, S. C.; Lin, T. L.; Yamauchi, K.; Hasegawa, H.; Hashimoto, T. Macromolecules 2001, 34, 671.
10. (a) Park, M.; Chaikin, P. M.; Register, R. A.; Adamson, D. H. Appl Phys Lett 2001, 79, 257; (b) Park, M.; Harrison, C.; Chaikin, P. M.; Register, R. A.; Adamson, D. H. Science 1997, 276, 1401.
11. (a) Cheng, J. Y.; Ross, C. A.; Chan, V. Z. H.; Thomas, E. L.; Lammertink, R. G. H.; Vancso, G. J. Adv Mater 2001, 13, 1174; (b) Cheng, J. Y.; Ross, C. A.; Thomas, E. L.; Smith, H. I.; Vancso, G. J. Appl Phys Lett 2002, 81, 3657.
12. (a) Lopes, W. A. Phys Rev E 2002, 65, 31606; (b) Lopes, W. A.; Jaeger, H. M. Nature 2001, 414, 735.
13. (a) Misner, M. J.; Skaff, H.; Emrick, T.; Russell, T. P. Adv Mater 2003, 15, 221; (b) Thurn-Aibrecht, T.; Schotter, J.; Castle, G. A.; Emley, N.; Shibauchi, T.; Krusin-Elbaum, L.; Guarini, K.; Black, C. T.; Touminen, M. T.; Russell, T. P. Science 2000, 290, 2126; (c) Kim, H. C.; Jia, X.; Stafford, C. M.; Kim, D. H.; McCarthy, T. J.; Tuominen, M.; Hawker, C. J.; Russell, T. P. Adv Mater 2001, 13, 795.
14. (a) Spatz, J. P.; Herzog, T.; Mobmer, S.; Ziemann, P.; Moller, M. Adv Mater 1999, 11, 149; (b) Mossmer, S.; Spatz, J. P.; Moller, M.; Aberle, T.; Schmidt, J.; Burchard, W. Macromolecules 2000, 33, 4791.
15. Sohn, B. H.; Choi, J. M.; Yoo, S. I.; Yun, S. H.; Zin, W. C.; Jung, J. C.; Kanehara, M.; Hirata, T.; Teranishi, T. J Am Chem Soc 2003, 125, 6368.
16. (a) Yue, J.; Sankaran, V.; Cohen, R. E.; Schrock, R. R. J Am Chem Soc 1993, 115, 4409; (b) Kane, R. S.; Cohen, R. E.; Silbey, R. Chem Mater 1999, 11, 90; (c) Sohn, B. H.; Cohen, R. E.; Papaefthymiou, G. C. J Magn Magn Mater 1998, 182, 21; (d) Abes, J. I.; Cohen, R. E.; Ross, C. A. Mater Sci Eng C 2003, 23, 641.
17. (a) Chan, Y. N. C.; Schrock, R. R. Chem Mater 1993, 5, 566; (b) Tassoni, R.; Schrock, R. R. Chem Mater 1994, 6, 744; (c) Fogg, D. E.; Radzilowski, L. H.; Blanski, R.; Schrock, R. R.; Thomas, E. L. Macromolecules 1997, 30, 417.
18. (a) Ahmed, S. R.; Kofinas, P. Macromolecules 2002, 35, 3338; (b) Ahmed, S. R.; Ogale, S. B.; Papaefthymiou, G. C.; Ramesh, R.; Kofinas, P. Appl Phys Lett 2002, 80, 1616.
19. (a) Moffitt, M.; Vali, H.; Eisenberg, A. Chem Mater 1998, 10, 1021; (b) Moffitt, M.; McMahon, L.; Pessel, V.; Eisenberg, A. Chem Mater 1995, 7, 1185.
20. Bockstaller, M. R.; Lapetnikov, Y.; Margel, S.; Thomas, E. L. J Am Chem Soc 2003, 125, 5276.
21. (a) Ribbe, A. E.; Okumura, A.; Matsushige, K.; Hashimoto, T. Macromolecules 2001, 34, 8239; (b) Hashimoto, T.; Harada, M.; Sakamoto, N. Macromolecules 1999, 32, 6867.
22. (a) Weng, C. C.; Wei, K. H. Chem Mater 2003, 15, 2936; (b) Yeh, S. W.; Wei, K. H.; Sun, Y. S.; Jeng, U. S.; Liang, K. S. Macromolecules 2003, 36, 7903; (c) Jeng, U. S.; Sun, Y. S.; Lee, H. Y.; Hsu, C. H.; Liang, K. S. Macromolecules 2004, 37, 4617.
23. (a) Urbas, A. M.; Maldovan, M.; DeRege, P.; Thomas, E. L. Adv Mater 2002, 14, 1850; (b) Bockstaller, M.; Olb, R.; Thomas, E. L. Adv Mater 2001, 13, 1783.
24. (a) Gao, M. Y.; Richter, B.; Kirstein, S. Adv Mater 1997, 9, 802; (b) Gao, M. Y.; Richter, B.; Kirstein, S.; Mohwald, H. J Phys Chem B 1998, 102, 4096.
25. (a) Thompson, R. B.; Ginzburg, V. V.; Matsen, M. W.; Balazs, A. C. Science 2001, 292, 2469; (b) Thompson, R. B.; Ginzburg, V. V.; Matsen, M. W.; Balazs, A. C. Macromolecules 2002, 35, 1060; (c) Lee, J. Y.; Shou, Z.; Balazs, A. C. Phys Rev Lett 2003, 91, 136103.
26. (a) Henglein, A. Chem Rev 1989, 89, 1861; (b) Veinot, J. G. C.; Ginzburg, M.; Pietro, W. J Chem Mater 1997, 9, 2117; (c) Herron, N.; Wang, Y.; Eckert, H. J Am Chem Soc 1990, 112, 1322; (d) Brus, L. J Phys Chem 1986, 90, 2555.
27. Chen, W. In Handbook of Nanostructured Materials and Nanotechnology; Nalwa, H. S., Ed.; Academic: New York; 1999; Chapter 5, pp 344–350.
28. Floudas, G.; Tsitsilianis, C. Macromolecules 1997, 30, 4381.
29. Qiao, J.; Yoshimoto, N.; Ishikawa, M.; Morita, M. Chem Mater 2003, 15, 2005.